Computer Simulation of Viscoelasticity in Polymer Melts

J. Gao and J. H. Weiner*

Division of Engineering and Department of Physics, Brown University, Providence, Rhode Island 02912

Received July 29, 1991; Revised Manuscript Received October 31, 1991

ABSTRACT: A method is presented for the simulation by molecular dynamics of stress relaxation in polymer melts. It is applied to dense model systems of short freely-jointed chains with repulsive excluded-volume interactions. Stress histories are fitted by a Prony series. The model parameters when subjected to Caswell-Paboojian scaling agree well with values observed for real systems. In contrast to the usual assumption, the shear stress is found to be due to the excluded-volume interactions and not to the forces in the covalent bonds of the chain. The utility of the entropic spring concept in the earlier stages of stress relaxation is also placed into question by these simulations.

(1) Introduction

We have been concerned for some time with the role of excluded-volume interactions in rubber elasticity and have used the computer simulation of idealized atomistic models as the principal tool in our studies.[1-3] The major conclusion we have been led to is that, contrary to the usual physical picture, excluded-volume interactions do not merely make a hydrostatic contribution to the stress. In fact, the deviatoric or anisotropic part of the stress in these materials arises, on the atomic level, mainly through these interactions. In this paper we examine the implications of this result for polymer systems undergoing nonequilibrium deformation processes.

To fix ideas and to motivate our approach, consider a step shear strain γ_0 applied at time $t = 0$ to a polymer melt at temperature $T = T_0$. If we assume that the theory of linear viscoelasticity applies, then the corresponding shear history $\tau(t)$ is given by

$$\tau(t) = \gamma_0 G(t) \tag{1}$$

where $G(t)$ is the shear relaxation modulus. It begins at a high value $G(0) = G_g$ corresponding to glassy behavior and decays to zero monotonically. If instead of a melt we conduct the experiment on a corresponding amorphous cross-linked system, the early time behavior is similar but $G(t)$ decays to $G_r > 0$, the equilibrium rubber shear modulus. If the same experiment is conducted at a temperature $T > T_0$, then the corresponding modulus $G_T(t)$ follows a similar history but at a more rapid rate. To good approximation it is found[4] that, for a given reference temperature T_0, there exists a constant factor a_T such that $G_T(t) = G_{T_0}(a_T t)$, with $a_T > 1$ for $T > T_0$.

On the atomistic level, this increase in the rate of decay of $G_T(t)$ is ascribed to the increase in atomic mobility at the higher temperature. This increase in mobility comes about for two reasons: The mean atomic speed increases as $T^{1/2}$, and, more importantly, the effect of thermal expansion (at constant pressure) leads to a more open or less densely packed system. The fact that time-temperature scaling works so well suggests that the same basic atomic mechanisms are operative at the different temperature levels but are occurring at different laboratory time rates as the atomic mobility changes.

This time-temperature equivalence is exploited in the laboratory by running experiments at different temperature levels in order to bring the different types of behavior, glassy, rubbery, etc., into the range of a convenient experimental time window. Although less convenient, it is also possible to change the time scale by altering the imposed pressure[5] and so varying the density of the system.

The same philosophy underlies our computer simulation experiments. Since our models are atomistic in character, the numerical time steps Δt employed in simulations is on the order of $\Delta t = 10^{-15}$ s. For reasonable expenditure of computer time we are therefore restricted to processes lasting, for the type of simulations here performed, on the order of 10^{-11} s, clearly a very short time scale as compared to the usual laboratory time scale, and some of the applied strain rates are on the order of 10^{10} s^{-1}. We attempt to circumvent these difficulties by using a model system in which the atomic mobility is very high because of the nature of the model chains, the packing fraction of the system, etc., so that the simulated relaxation modulus decays substantially (through 2 or 3 orders of magnitude) in a given computer simulation. Although we have thus time-shifted the phenomena into an ultra-short time window, we hope, as in laboratory time shifting, that the basic atomic mechanisms revealed by our model retain some validity for real systems. As we shall see, the scaling properties of our results give us some confidence that this may be the case. We may also note that experiments conducted in a convenient laboratory time window are sometimes interpreted, through the time-temperature equivalence concept, as descriptive of behavior in the time frame of our calculations.[6]

There appears to have been little use of computer simulation on the atomic level to study nonequilibrium deformation processes in polymeric systems. One exception is the recent work of Brown and Clarke,[7] who utilized a realistic atomistic model for a polymeric solid and simulated a constant tensile stress increase at different temperature levels. Their simulations show many similarities to the behavior of real materials.

Our simulations involve the imposition of constant strain rate rather than constant stress rate. By comparing simulations at different strain rates we are able to check the extent to which our model system may be analyzed on the basis of linear viscoelasticity. Details of the simulation procedure and the means of determination of the shear relaxation modulus are given in section 2. Results are presented in section 3 and are discussed in section 4. Conclusions and directions for future work are contained in section 5.

(2) Computer Simulation Procedure

Chain Model. We use in this paper, as in much of our previous work, a simple chain model that has both the covalent bonding characteristic of macromolecules and

0024-9297/92/2225-1348$03.00/0

the attribute of excluded volume. It approximates the hard-sphere, freely-jointed chain. For computational and conceptual convenience the covalent potential is represented by a stiff linear spring and the hard-sphere potential is replaced by the repulsion part of the Lennard-Jones potential. That is, the covalent potential $u_c(r)$ is

$$u_c(r) = \frac{1}{2}\kappa(r-a)^2 \tag{2}$$

where r is the distance between adjacent atoms on a given chain and a is the zero-force bond length; the noncovalent potential is

$$\begin{aligned} u_{nc}(r) &= 4\epsilon[(\sigma/r)^{12} - (\sigma/r)^6] \quad \text{for } r \le r_0 \\ &= u_{nc}(r_0) \quad \text{for } r \ge r_0 \end{aligned} \tag{3}$$

where r denotes the distance between any adjacent pair of atoms on a given chain or between any pair of atoms on different chains and $r_0 = 2^{1/6}\sigma$. The results reported in this paper were all carried out, except as noted, for $\sigma = a$, $\kappa a/kT_0 = 200$, and $\epsilon/kT_0 = 0.75$. For these parameter values, the bond length undergoes only small fractional changes and σ may be regarded as an effective hard-sphere diameter. Each chain has N bonds and $N+1$ atoms. The reference time unit used in our simulation is $t_0 = (m/\kappa)^{1/2}$ where m is the monomer mass. For the above parameter values, we may also write $t_0 = 0.071(m\sigma^2/kT_0)^{1/2}$. For m and σ corresponding to the CH_2 monomer and $T_0 = 300$ K, $t_0 = 7.2 \times 10^{-14}$ s.

Melt Model. The simulation is carried out using periodic boundary conditions as is customary in molecular dynamics simulation. The basic cell, referred to a rectangular Cartesian coordinate system x_1, x_2, x_3, is a rectangular parallelepiped with dimensions L_1, L_2, and L_3 in the coordinate directions. There are ν chains per basic cell. This leads to a reduced density

$$\rho = n\sigma^3/v \tag{4}$$

where $n = \nu(N+1)$ and $v = L_1L_2L_3$. We use as a fixed reference volume $v_0 = 1008\sigma^3$, corresponding to $\rho = 1.0$ for $\nu = 48$ chains and $N = 20$.

In most of the simulations all atoms of the chains are free to undergo thermal motion. In some simulations, described in section 4, chain vectors are held fixed, as in the oriented melt model introduced in ref 2.

Constant-Temperature Algorithm. In order to maintain a constant temperature in the melt during deformation, we employ the velocity scaling algorithm due to Berendsen, Postma, and van Gunsteren[8] and employed also by Brown and Clarke[7] in their simulations. We refer to the paper by Berendsen et al. for the motivation of their procedure. The final algorithm for the determination of the atomic position $\mathbf{x}(t+\Delta t)$ in terms of the earlier positions $\mathbf{x}(t)$ and $\mathbf{x}(t-\Delta t)$ takes the form

$$\mathbf{x}(t+\Delta t) = \mathbf{x}(t) + \xi\left(\mathbf{v}\left(t-\frac{1}{2}\Delta t\right) + \frac{\mathbf{f}}{m}\Delta t\right)\Delta t \tag{5}$$

where

$$\mathbf{v}\left(t-\frac{1}{2}\Delta t\right) = (\mathbf{x}(t) - \mathbf{x}(t-\Delta t))/\Delta t \tag{6}$$

the force $\mathbf{f}$ acting on the atom in question is determined from atomic positions at time t, and velocity scaling factor

$$\xi = \left[1 + \frac{\Delta t}{\tau_T}\left(\frac{T_0}{T\left(t-\frac{1}{2}\Delta t\right)} - 1\right)\right]^{1/2} \tag{7}$$

where the temperature $T(t-{}^1/_2\Delta t)$ is based on the atomic velocities at $t-{}^1/_2\Delta t$ as computed from eq 6. Appropriate values of the parameter τ_T are discussed by Brown and Clarke.[9] In our simulations involving high strain rates we generally found it necessary to use $\tau_T = 20\Delta t \sim 40\Delta t$. Because the stress history in our simulation proceeds at widely varying rates during a given simulation, we used different values of the time step Δt during it. An example of the type of schedule used is shown in Figure 1.

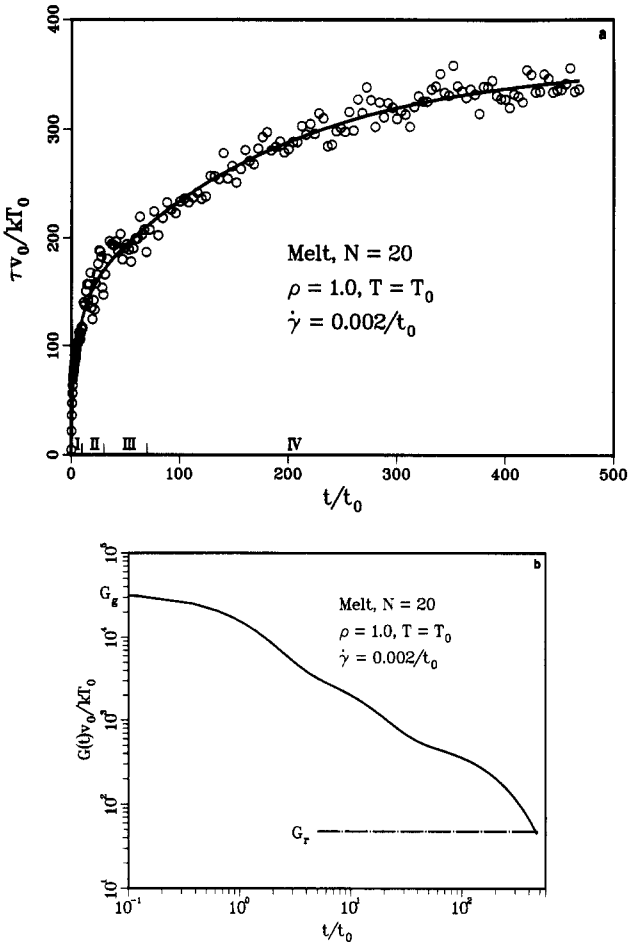

Figure 1. (a) Shear stress history $\tau(t)$. The schedule of numerical time steps employed is as follows: period I, $\Delta = 0.0125t_0$; II, $\Delta = 0.025t_0$; III, $\Delta = 0.05t_0$; IV, $\Delta = 0.1t_0$. The curve represents the fit to data on the basis of the Prony series, eq 17; parameters are listed in Table I. (b) Corresponding shear relaxation modulus, $G(t)$, eq 16. The value of the ideal rubber modulus shown is computed on the basis of $G_r = \nu kT_0/v_0$. With $\sigma = 4.28$ Å, corresponding to the CH_2 monomer, and with $T_0 = 300$ K, $kT_0/v_0 = 0.053$ MPa.

Virial Stress Formula. For the case in which all interactions are through pair potentials, the generalized virial formula takes the form[1]

$$vt_{ij} = -n_t kT\delta_{ij} + \sum\langle r_\alpha^{-1}u'_\alpha(r_\alpha)r_{\alpha i}r_{\alpha j}\rangle \tag{8}$$

where, in addition to previously defined quantities, v is the volume of the system, t_{ij} are the components of the stress tensor (force per unit present area) referred to the fixed rectangular Cartesian system x_i, $i = 1$–3, n_t is the number of atoms free to undergo thermal motion, δ_{ij} is the Kronecker delta, α ranges over all pairs of atoms, $\mathbf{r}_\alpha$ is the vector displacement between the α pair with components $r_{\alpha i}$, $r_\alpha = |\mathbf{r}_\alpha|$, $u_\alpha(r_\alpha)$ is the pair potential acting between the α pair, $u'_\alpha = du_\alpha/dr_\alpha$, and brackets denote long-time averages. We may also rewrite eq 8 to make the two types

of interactions u_c and u_{nc} explicit as

$$vt_{ij} = -n_v kT\delta_{ij} + \sum_{\alpha\in c}\langle r_\alpha^{-1}u'_c(r_\alpha)r_{\alpha i}r_{\alpha j}\rangle + \sum_{\alpha\in nc}\langle r_\alpha^{-1}u'_{nc}(r_\alpha)r_{\alpha i}r_{\alpha j}\rangle \quad (9)$$

where the notations $\alpha \in c$ or $\alpha \in nc$ indicate that the sums range over all pairs of covalently or noncovalently interacting atoms, respectively.

Deformation Procedure. In order to determine the shear relaxation modulus $G(t)$, we find it convenient to simulate the system subjected to a constant shear rate $\dot\gamma$ for $t > 0$. By application of the principles of linear viscoelasticity,[4] the corresponding shear stress history $\tau(t)$ is

$$\tau(t) = \dot\gamma\int_0^t G(t')\,dt' \quad (10)$$

so that

$$G(t) = \dot\tau(t)/\dot\gamma \quad (11)$$

where, as usual, the superposed dot denotes the time derivative.

The direct imposition of a shear strain γ on the basic cell would require the use of a nonrectilinear lattice for the periodic boundary conditions. To avoid this, we impose a state of pure shear with respect to the coordinate system x_1, x_2, x_3 in which the basic cell has dimensions L_1, L_2, and L_3 with $L_1 = L_2 = L_3 = L$ in the reference state. We begin by recalling the basic relations between pure and simple shear. A pure shear corresponds to a change of basic cell dimension by the relations

$$L_1 = \lambda L,\quad L_2 = L,\quad L_3 = \lambda^{-1}L \quad (12)$$

This pure shear deformation, together with a suitable rotation,[10] corresponds to a simple shear γ where

$$\gamma = \lambda - \lambda^{-1} \quad (13)$$

so that

$$\lambda = (\gamma + (\gamma^2 + 4)^{1/2})/2 \quad (14)$$

If t_{ij} is the state of stress referred to the x_1, x_2, x_3 coordinate system in which the deformation is pure shear, the shear stress $\tau_{13} = \tau$ in the coordinate system x'_1, x'_2, x'_3 in which the deformation is simple shear is

$$\tau = \frac{\lambda}{1+\lambda^2}(t_{11} - t_{33}) \quad (15)$$

The kinematical relation between pure and simple shear leads to the result[10] that the angle between the x_1 and x'_1 axes varies with γ. Our simulations are limited to $\gamma \le 1$, and this corresponds to a maximum variation of this angle of $\sim 13°$, a variation which should have little effect.

In the simulation we impose a constant simple shear rate $\dot\gamma$ for $t > 0$. The value of $\lambda(t)$ is then obtained from eq 14 with $\gamma = \dot\gamma t$. At that time, $t_{11}(t)$ and $t_{33}(t)$ are obtained by use of the virial equation, eq 9, with all quantities referred to the x_1, x_2, x_3 system. Then $\tau(t)$ is obtained from eq 15.

Note that the deformation is imposed solely by change of the dimensions of the basic cell as in eq 12. The deformation is transmitted to the atoms of the system only through the resultant change in periodic boundary conditions; in particular, no scaling of atomic coordinates is employed. Therefore, to use the terminology of Evans and Morriss,[11] our simulations use a boundary-driven algorithm. In treating molecular liquids this approach may pose a problem regarding the transfer of the deformation to particles in the cell interior and algorithms, such as the SLLOD method,[11] have been developed for applying a constant strain rate to the system. However we are dealing with a stiff system with high wave propagation speeds, and calculations show that the time required for molecules in the interior of the cell to sense boundary motion is negligibly small compared to the deformation rate. As a check that conditions in the cell interior are effectively uniform, a simulation was performed with reduced cell size, as reported in the following.

Initial Configuration. Because of the fluctuations inherent in the small size of the system, the initial stress $t_{ij}(0)$ is nonzero in an arbitrarily selected initial configuration. For this reason it is necessary to repeat the simulations n' times, using n' independent initial configurations and then averaging the results to obtain $t_{ij}(t)$.

Independent initial configurations are obtained in the following manner: A simulation of the melt with $\dot\lambda = 0$ is performed and the time correlation function $\langle \mathbf{R}(t)\cdot\mathbf{R}(0)/R^2(0)\rangle = \phi(t)$ is calculated, where $\mathbf{R}(t)$ is a chain vector and the average is over all of the chains of the system. For melts of chains with $N \le 10$ bonds, configurations separated by a time interval t', where $\phi(t') \approx 0.1$, are regarded as independent; at these time intervals, all atom positions and velocities are stored to be used as initial conditions for the simulations. (For melts with $N = 20$, to avoid excessive computer time, we used configurations separated by the time interval t', where $\phi(t') \approx 0.5$.) Two additional sets of initial conditions were effectively obtained from each by permuting the coordinate directions in the imposition of the deformation, eq 12. For the results reported here we used $n' = 120$. This large number of repeated calculations was found necessary because of the high rate of change of $\tau(t)$ at early times and the consequent need to average stress over very short time intervals.

Computation of $G(t)$. As is customary in this field, we express $G(t)$ as a Prony series, that is, in the form

$$G(t) = \sum_{i=1}^{N'} g_i e^{-t/\lambda_i} \quad (16)$$

For this purpose it is necessary to determine the constants g_i and λ_i to fit the simulated values of $\tau(t)$ by an expression of the form

$$\tau(t) = \dot\gamma\sum_{i=1}^{N'}\lambda_i g_i(1 - e^{-t/\lambda_i}) \quad (17)$$

where $\dot\gamma$ is the imposed constant strain rate for the simulation. The number N' of the modes in the Prony series is chosen to provide approximately one mode per decade of time[12] covered by the simulation. A least-squares nonlinear fitting procedure is then used to determine all of the constants g_i and λ_i simultaneously, subject to the constraint of fixing the initial value of $\dot\tau(0)$. Both Monte Carlo and Levenberg–Marquardt[13] fitting algorithms were used; the former was found most effective in avoiding local minima although it requires somewhat more computer time. In some cases, fits were made for both $N' = 3$ and $N' = 4$ modes, with a final choice based on goodness of fit to the $\tau(t)$ history. In other cases, two of the modes for $N' = 4$ were found to be essentially identical and the result proved equivalent to the $N' = 3$ mode selection.

(3) Results

A typical result for the stress history $\tau(t)$ in a polymer melt corresponding to a constant strain rate $\dot\gamma$ as obtained by computer simulation is shown in Figure 1a. It is seen that the scatter in the computed points is initially very small but grows with time. This is a reflection of the growth

Table I
Simulation Data[a]

data no. 1 (Figure 1)	data no. 2 (Figure 2)
$N = 20, \nu = 48, \rho = 1.0$ $T = T_0, \dot\gamma = \dot\gamma_0, G_g = 1830$ $\lambda_1 = 0.075, \lambda_2 = 0.70, \lambda_3 = 12.9$ $g_1 = 1586, g_2 = 211.3, g_3 = 32.95$	$N = 20, \nu = 48, \rho = 1.0$ $T = T_0, \dot\gamma = 0.5\dot\gamma_0, G_g = 1831$ $\lambda_1 = 0.078, \lambda_2 = 0.43, \lambda_3 = 13.7$ $g_1 = 1574, g_2 = 218.5, g_3 = 38.30$
data no. 3 (Figure 4)	**data no. 4 (Figure 4)**
$N = 20, \nu = 48, \rho = 1.1$ $T = T_0, \dot\gamma = \dot\gamma_0, G_g = 2488$ $\lambda_1 = 0.081, \lambda_2 = 0.63, \lambda_3 = 4.49,$ $\lambda_4 = 70.4$ $g_1 = 2020, g_2 = 349.7, g_3 = 100.9,$ $g_4 = 17.85$	$N = 20, \nu = 48, \rho = 1.2$ $T = T_0, \dot\gamma = \dot\gamma_0, G_g = 3331$ $\lambda_1 = 0.079, \lambda_2 = 1.57,$ $\lambda_3 = 19.9$ $g_1 = 2500, g_2 = 754.3,$ $g_3 = 76.69$
data no. 5 (Figure 7)	**data no. 6 (Figure 5)**
$N = 20, \nu = 48, \rho = 1.0$ $T = 0.5T_0, \dot\gamma = \dot\gamma_0, G_g = 1645$ $\lambda_1 = 0.079, \lambda_2 = 1.09, \lambda_3 = 15.3$ $g_1 = 1367, g_2 = 243.6, g_3 = 34.67$	$N = 10, \nu = 96, \rho = 1.0$ $T = T_0, \dot\gamma = \dot\gamma_0, G_g = 1796$ $\lambda_1 = 0.058, \lambda_2 = 0.27, \lambda_3 = 5.91,$ $\lambda_4 = 10.3$ $g_1 = 1271, g_2 = 475.7, g_3 = 20.76,$ $g_4 = 27.71$
data no. 7 (Figure 5)	**data no. 8 (Figure 3)**
$N = 5, \nu = 144, \rho = 1.0$ $T = T_0, \dot\gamma = \dot\gamma_0, G_g = 1863$ $\lambda_1 = 0.071, \lambda_2 = 0.12, \lambda_3 = 1.59,$ $\lambda_4 = 7.44$ $g_1 = 1082, g_2 = 701.8, g_3 = 42.36,$ $g_4 = 36.72$	simple fluid, 1008 atoms, $\rho = 1.0$ $T = T_0, \dot\gamma = \dot\gamma_0, G_g = 2157$ $\lambda_1 = 0.056, \lambda_2 = 0.25$ $g_1 = 1452, g_2 = 704.9$

[a] Units employed are as follows: λ_i (i = 1–4), 10^{-12} s; g_i (i = 1–4), G_g, MPa; T_0 = 300 K; $\dot\gamma_0 = 0.002/t_0 = 2.78 \times 10^{10}$ s^{-1} with $t_0 = 7.2 \times 10^{-14}$ s.

of atomic displacements due to thermal motion. The corresponding value of the stress relaxation modulus $G(t)$ is shown in Figure 1b. Values of the parameters g_i and λ_i obtained through the fitting of $\tau(t)$ for this calculation, as well as for other simulations reported here, are listed in Table I. As a measure of the scatter from the fitted $\tau(t)$, we computed the quantity $\Delta = t_f^{-1}\int_0^{t_f}|\Delta\tau|/\tau\, dt$, where $\Delta\tau(t)$ is the difference between the simulated value of $\tau(t)$ and the fitted value and t_f is the total time of the simulation. We find Δ = 0.03–0.04 for all of the simulations except for data no. 2 (Table I); for the latter, run at half strain rate and consequently half stress level, $\Delta \simeq 0.07$.

Effect of Strain Rate. It is necessary to carry out these simulations at high strain rates; otherwise, the stress levels are too low and the results are obscured by the scatter. To check on the effect of the strain rate, a second simulation was performed under conditions corresponding to those in Figure 1, but at half the strain rate; the results are compared in Figure 2 where the data points are omitted and only the fitted curves shown. It is seen that at early times the value of $\tau(t)/\dot\gamma$ are indeed independent of $\dot\gamma$ and thus fit into the framework of linear viscoelasticity. However, for later times, $\tau(t)/\dot\gamma$ is lower for the higher strain rate; this corresponds to the phenomenon of shear thinning.

Simple Fluid. We have also performed a simulation of the simple fluid obtained from the polymer melt model by the removal of all covalent bonds. The results are shown in Figure 3. As seen from the numerical values in Table I, the two modes needed to fit the simple fluid data have parameters that are close in numerical value to the two lowest modes for the polymer melt. The value of the viscosity, η_0, for the simple fluid is in reasonable agreement with the values for a hard-sphere liquid at the same reduced density.[14]

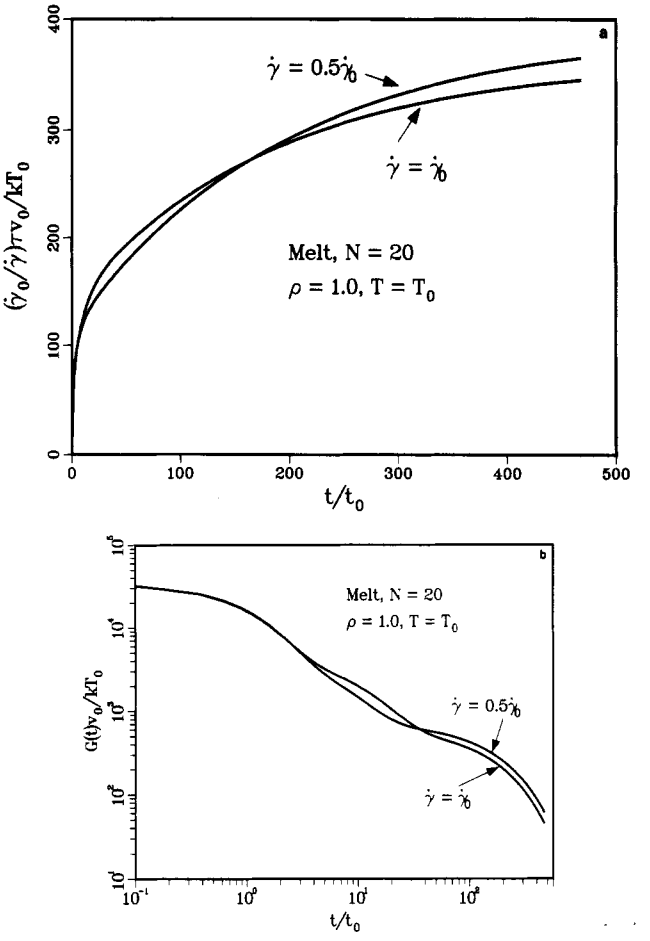

Figure 2. Effect of strain rate for conditions shown in Figure 1. $\dot\gamma_0 = 0.002/t_0$. (a) Stress history $\tau(t)$ scaled by the imposed strain rate. Curves fitted to data on the basis of the Prony series. (b) Corresponding shear relaxation modulus, $G(t)$.

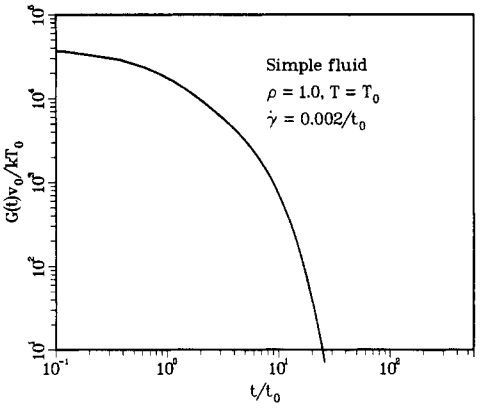

Figure 3. Shear relaxation modulus, $G(t)$, for a simple fluid with 1008 atoms in volume v_0.

Effect of ρ. Simulations were run for reduced density ρ = 1.0, 1.1, and 1.2 with all other parameters fixed. The resulting behavior of $G(t)$ is shown in Figure 4. The expected slowing-down of the relaxation with increased packing may be noted.

Effect of Chain Length. Simulations were carried out for chains with N = 5, 10, and 20 bonds. Results are shown in Figure 5. The effect of chain length becomes significant only at later times.

Chain Vector Deformation. The program computes $\langle R^2(t)\rangle$, where the mean is computed at each time step over all of the chains of the system. Typical results are shown in Figure 6. They are compared there with the variation predicted under the assumption that the chain

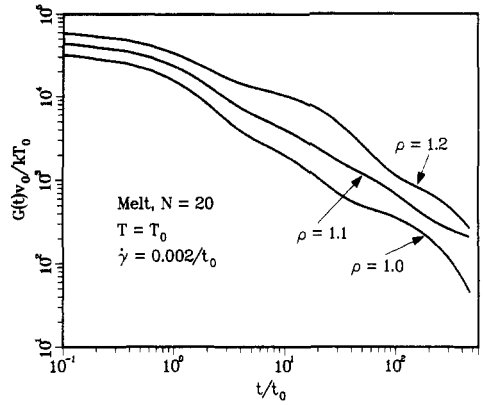

Figure 4. Effect of reduced density ρ, eq 4. Shear relaxation modulus, $G(t)$, for three reduced densities.

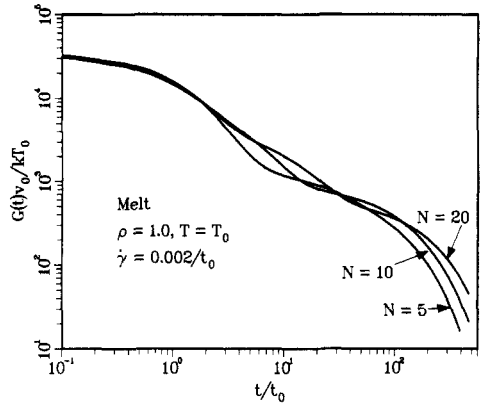

Figure 5. Effect of chain length, N. Shear relaxation modulus, $G(t)$, for three values of N.

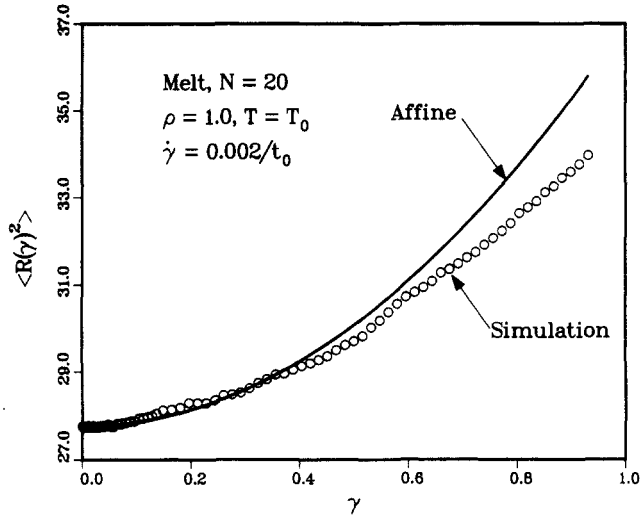

Figure 6. Mean-squared chain vector, $\langle R^2 \rangle$, averaged over all chains of the system as a function of total shear deformation γ.

vectors are initially isotropically distributed and undergo the same affine deformation that is applied to the basic cell. It is seen that the observed variation is reasonably consistent with this assumption. Our simulations show that this agreement improves with increasing melt density.

Effect of Temperature at Constant ρ. One simulation, was run at $T = 0.5T_0$, with all other parameters held fixed. The resulting values of $G(t)$ are shown in Figure 7. Although there is a small degree of slowing of the stress relaxation upon the drop in temperature, it is seen that when the reduced density is held fixed, this effect is small.

Caswell–Paboojian Scaling. In a recent paper, Caswell and Paboojian[15] have introduced scaled Prony

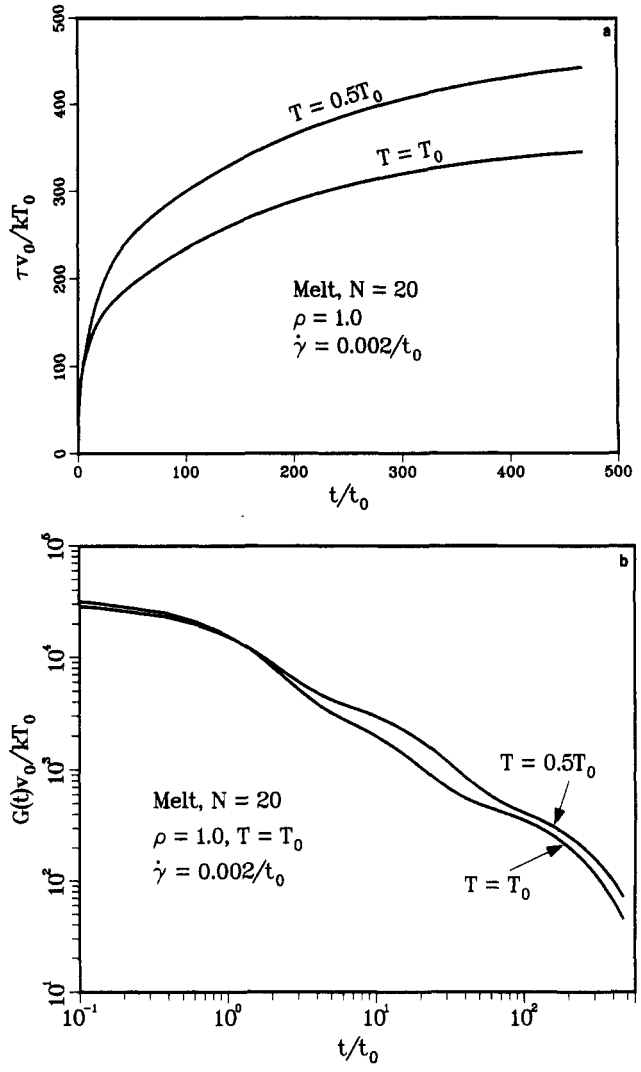

Figure 7. Effect of temperature at fixed density ρ. (a) Stress history. (b) Corresponding shear relaxation modulus, $G(t)$.

series parameters $\bar{g}_i$ and $\bar{\lambda}_i$ defined as follows:

$$\bar{g}_i = g_i J_0 \tag{18}$$

$$\bar{\lambda}_i = \lambda_i / \lambda_0 \tag{19}$$

The scaling parameters J_0 and λ_0 are defined in terms of the original series as follows:

$$\eta_0 = \int_0^\infty G(t)\, dt \approx \sum_{i=1}^{N'} g_i \lambda_i \tag{20}$$

$$\lambda_0 \eta_0 = \int_0^\infty tG(t)\, dt \approx \sum_{i=1}^{N'} g_i \lambda_i^2 \tag{21}$$

$$J_0 = \lambda_0 / \eta_0 \tag{22}$$

They have shown that a large number of data based on the Prony series fits to experiments on both polymer melts and polymers in solution are reduced, with small scatter, to a single $\bar{g}$, $\bar{\lambda}$ curve when scaled as in eqs 18 and 19. They caution against using data from experiments performed over too short a time scale since then the scaling constants as obtained from eqs 20 and 21 are inaccurate. Although this is the case for our simulation data, and with this caveat in mind, we nevertheless scale then in this manner and show the results in Figure 8. Shown also in this figure are

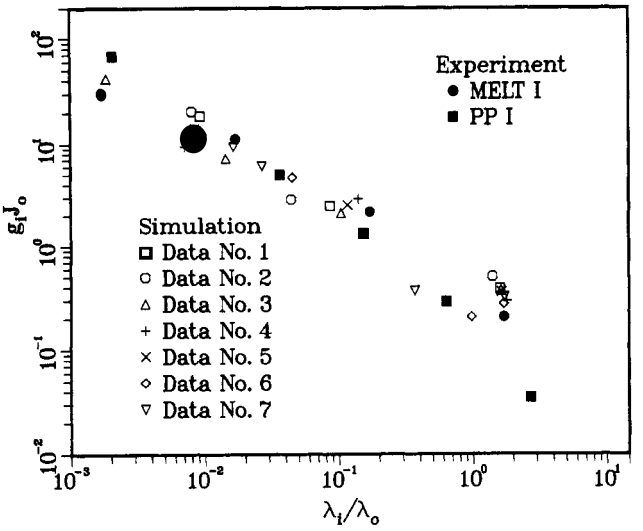

Figure 8. Caswell–Paboojian scaling of simulation results (open symbols) and of experimental results for selected systems (filled symbols). Sources of experimental data for melt I (polyethylene) and PP I (polypropylene) and additional experimental results subjected to the same scaling may be found in ref 15.

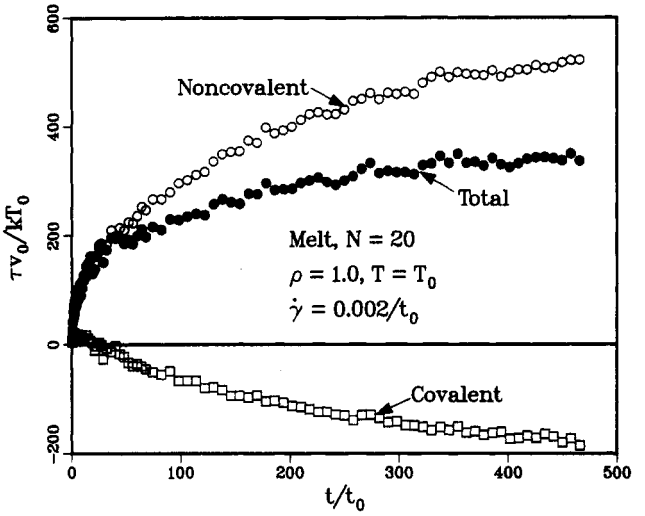

Figure 9. Noncovalent (excluded-volume) and covalent contributions to the shear stress τ, for conditions as in Figure 1.

some of the scaled experimental data from the paper by Caswell and Paboojian.[15]

Covalent and Noncovalent Contribution to Stress. The simulation program also records the separate contributions to the shear stress τ by the covalent interactions, u_c, and the noncovalent, excluded-volume interaction, u_{nc}. The results for a typical set of parameters are shown in Figure 9. It is seen that the shear stress is primarily due to excluded-volume interactions. In fact, except at very early times, the covalent contribution is negative. As in our previous work on equilibrium rubber elasticity,[1-3] the negative covalent contribution may be traced to the fact that, at these densities, the covalent bonds are in compression.

Glass Modulus. The simulations provide accurate values for the glass modulus $G_g = G(0)$. Numerical results are given in Table I. It is of interest to note that the value G_g shows little dependence on N, the number of bonds in the chains, and that the value of G_g for the simple fluid is slightly larger than that for the corresponding melt.

Effect of System Size. As a check that the size of the system simulated is adequate, a simulation was performed for the case shown in Figure 1, but with half the number of chains in the basic cell and with the cell dimensions reduced to maintain ρ constant. The result for $G(t)$ for this simulation was in excellent agreement with that shown in Figure 1b for the larger system. In particular, the value of $G(t)$ for the half-size system was close to indistinguishable, on the scale of that figure, from that full-size system. As discussed previously, this result demonstrates that ample time is available in the full-size system for the communication of the deformation from the boundary to the cell interior.

(4) Discussion

One of the principal results of the simulations of our polymer melt model is that the shear stress developed in the constant strain rate deformation arises primarily from the excluded-volume interactions between the atoms; the covalent bond contributions to the shear stress are actually negative. This result for nonequilibrium loading parallels that previously obtained by us for simulations corresponding to equilibrium rubber elasticity.

Atomic Ordering. It is easiest to describe the process whereby the spherically-symmetric excluded-volume interaction produces a shear stress in terms of pure shear in the x_1, x_2, x_3 coordinate system. As outlined in eq 12, the basic cell is being expanded in the x_1 direction and contracted in the x_3 direction at rates corresponding to constant $\dot{\gamma}$. In order to continue to meet packing requirements, an increase in ordering[16] is imposed on the atom distribution that gives rise to decreased repulsive interactions in the x_1 direction and increased interactions in the x_3 direction, i.e., to an algebraic increase in $t_{11}-t_{33}$ and therefore to an increase in τ (eq 15). Theoretically, this change in ordering could be described in terms of an anisotropic pair correlation function, that is, a function $g(\mathbf{r})$ proportional to the probability density of finding an atom at displacement $\mathbf{r}$ from an arbitrary atom of the system.[17] However, because of the steepness of the repulsive potential $u_{nc}(r)$, eq 3, the changes in $g(\mathbf{r})$ that are sufficient to give rise to the observed stresses would be difficult to detect and represent. Rather, we take the values of the stresses t_{11} and t_{33} themselves, as computed from the virial expression, eq 9, as both evidence and measures of this atomic ordering.

Maxwell Body. In the previous section we employed a Prony series, eq 16, to represent the shear relaxation function $G(t)$. This series represents, of course, a set of Maxwell bodies in parallel. We consider here, for simplicity, a single Maxwell body described by the differential relation

$$\frac{1}{g}\dot{\tau} + \frac{1}{\eta}\tau = \dot{\gamma} \tag{23}$$

or

$$\dot{\tau} = g\dot{\gamma} - \tau/\lambda^* \tag{24}$$

where $\lambda^* = \eta/g$.

For a constant strain rate experiment, as we have here simulated, this equation ascribes the rate of increase in the shear stress to two causes: an elastic part $g\dot{\gamma}$ proportional to the shear rate and a viscous part $-\tau/\lambda^*$ proportional to the stress.[18] The simulations serve to motivate an atomistic interpretation of these two contributions. (a) The elastic term, $g\dot{\gamma}$, is due to the increase in atomic ordering which is proportional to $\dot{\gamma}$. (b) At the same time, atomic thermal motion acts to oppose this increase in order. This disordering rate is, in first approximation, proportional to τ, since τ is a measure of the ordering that has been produced. We may further motivate the dependence of the disordering rate on τ by the following

considerations. For these dense systems we expect that extensive atomic displacements will require passage over energy barriers with rates governed by an Arrhenius type of relation. The stress τ will facilitate passage over a barrier in a direction that decreases τ and impede passage in the reverse direction. Schematically we can then represent the net rate f of passage over a given barrier of height E_b as

$$\begin{aligned} f &= \nu[e^{-\beta(E_b-\tau v_a)} - e^{-\beta(E_b+\tau v_a)}] \\ &= 2\nu \sinh(\beta\tau v_a) e^{-E_b/kT} \\ &\approx 2\nu\beta v_a \tau e^{-E_b/kT} \end{aligned} \tag{25}$$

where here ν denotes a frequency factor, v_a is an activation volume, $\beta = (kT)^{-1}$, and we have assumed in the final step that $\beta v_a \tau \ll 1$.

Role of Chains. Thus far we have not mentioned the chain structure that serves to distinguish a polymer melt from a simple fluid. The basic mechanisms we have described apply equally to both. The important role played by the covalent structure of the chains in a melt is greatly to reduce atomic mobility and thus to slow the disordering rate. This is illustrated by a simulation corresponding to a strain rate history

$$\dot\gamma = \dot\gamma_0 \quad \text{for } 0 < t < t_1$$

$$\dot\gamma = 0 \quad \text{for } t > t_1 \tag{26}$$

applied both to our model polymer melt and to the corresponding simple fluid obtained by omitting all covalent bonds. The results, shown in Figure 10, demonstrate the basic similarity in the two processes together with the large disparity in time scales.

In addition to that just described, the chains play another role. As we have seen, as the melt is subjected to a constant strain rate $\dot\gamma$, the chain vectors are deformed in a manner reasonably well-described by the corresponding affine deformation. This change in the chain vectors produces an additional change in atomic ordering that goes beyond that produced by γ in the simple liquid.

Consider first the situation in a cross-linked system deformed by a shear strain γ and in equilibrium, so that the theory of rubber elasticity applies, and assume that junctions do not undergo thermal motion and are deformed affinely. In previous simulations[3] we have shown that the deviatoric stress in such systems may be obtained from an expression of the form

$$t_{ij} = \frac{1}{v}\sum_{\beta} f_i(\beta)\, R_j(\beta) \tag{27}$$

where $R_j(\beta)$ are the components of the chain vector of chain β, $f_i(\beta)$ are the components of the chain force, and the sum is over all of the chains.

In the classical molecular theory of rubber elasticity, excluded-volume effects are completely neglected in computing the deviatoric stress and the chain force is calculated for ideal chains. If we further assume Gaussian chains, eq 27 then leads directly to the familiar results of the classical theory. We have shown in a previous paper[3] that, with suitable definition of the chain force, eq 27 may be employed as well in the presence of excluded-volume interaction and that the result differs only slightly from that obtained by use of the ideal force–length relation for the chains. We now examine the validity of this procedure for a polymer system undergoing a nonequilibrium deformation.

For this purpose we simulate a polymer melt undergoing the strain rate history of eq 26. In order to make contact

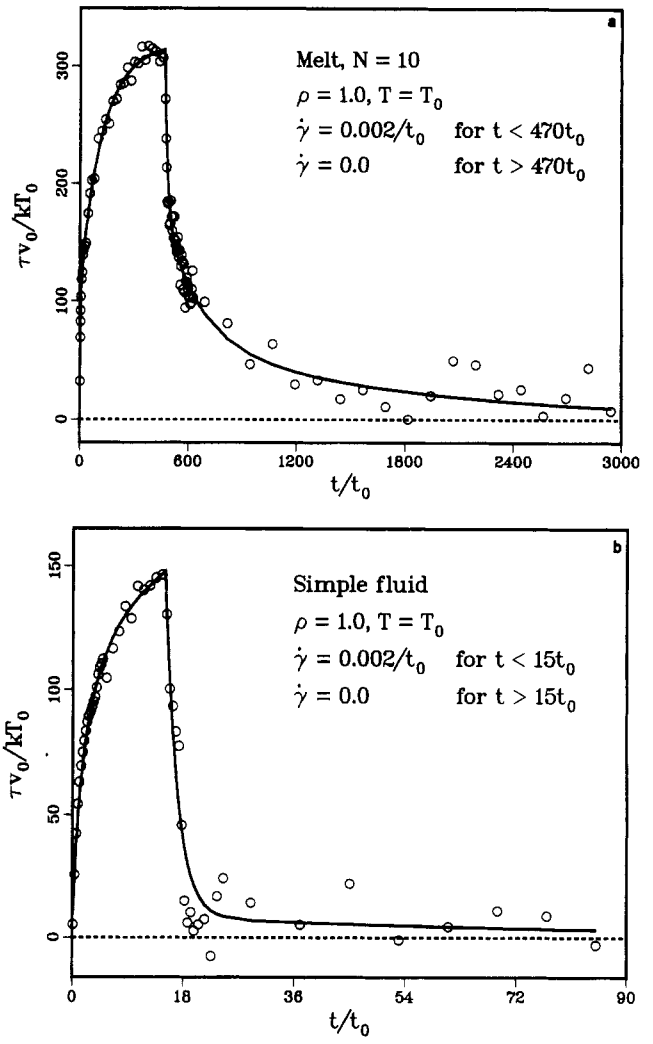

Figure 10. Loading and unloading stress histories for (a) a polymer melt and for (b) the corresponding simple fluid. After time $t = 630t_0$, the simulation for the melt is continued for only 6 of the initial 120 configurations and data averaged over longer time periods in order to permit extension to longer times. Note the difference in time scales.

with equilibrium rubber elasticity theory, we also fix the chain vectors[2] for $t > t_1$, although they are free to vary for $t < t_1$. Physically, we may think of this procedure as equivalent to instantaneous end cross-linking at time t_1.

In the simulation, we compute the chain force $\mathbf{f}(\beta)$ acting on the atom β by two methods: by use of the ideal force–length relation appropriate for short chains and by use of the virial chain force formula of ref 3 which is valid for interacting systems of chains. This expression, derived on the basis of equilibrium statistical mechanics, takes the form (the summation convention on double indices is not used here)

$$f_i(\beta)\, R_i(\beta) = -(N-1)kT + \sum_{\alpha\in c}\langle f_{\alpha i} r_{\alpha i}\rangle + \sum_{\alpha\in \text{intra}}\langle f_{\alpha i} r_{\alpha i}\rangle + \sum_{\alpha\in \text{inter}}\langle f_{\alpha i} x_{\alpha i}\rangle \tag{28}$$

where

$$f_{\alpha i} = u'_\alpha(r_\alpha)\frac{r_{\alpha i}}{r_\alpha} \tag{29}$$

with $u_\alpha = u_c$ in the first sum and $u_\alpha = u_{nc}$ in the latter two sums; $\alpha \in c$ indicates the sum over all covalent bonds in chain β, $\alpha \in$ intra indicates the sum over all intrachain pairs in noncovalent interaction with both atoms in the

pair belonging to chain β, and $\alpha \in$ inter indicates the sum over all interchain pairs where one atom in the pair α belongs to chain β. Here, $x_{\alpha i}$ are the components of the displacement vector from an end atom of chain β to that atom of chain β in the interchain pair α.

The results of this simulation are shown in Figure 11. Consider first the result of using eq 27 with $\mathbf{f}(\beta)$ based on the ideal chain force–length relation.[19] It is seen that this procedure greatly underestimates the stress during the nonequilibrium portion of the process. Only when equilibrium is reached are the stresses computed on the basis of the ideal chain force in substantial agreement with those based on the atomic virial formula, eq 8. This demonstrates that, during the nonequilibrium portion of the process, the stress is primarily due to the atomic ordering induced by the strain rate $\dot{\gamma}$, with the atomic ordering due to the affine deformation of chain vectors playing a secondary role. Only when the first atomic ordering is dissipated during the period $t > t_1$ with $\dot{\gamma} = 0$ do the two methods of stress computation come into reasonable agreement.

The behavior of the stress computed on the basis of eq 27 with $\mathbf{f}(\beta)$ determined from the simulation by use of the virial chain force formula, eq 28, makes another interesting point. The virial force formula responds to the actual atomic ordering induced by the change in the chain vector. As seen from the results in Figure 11, time is required for the development of the atomic ordering due to this cause. For this reason, the stress based on eq 27 with $\mathbf{f}(\beta)$ determined from eq 28 lags the result based on the ideal force–length relation. Again, only when equilibrium is reached do all three methods lead to values of the stress in substantial agreement.

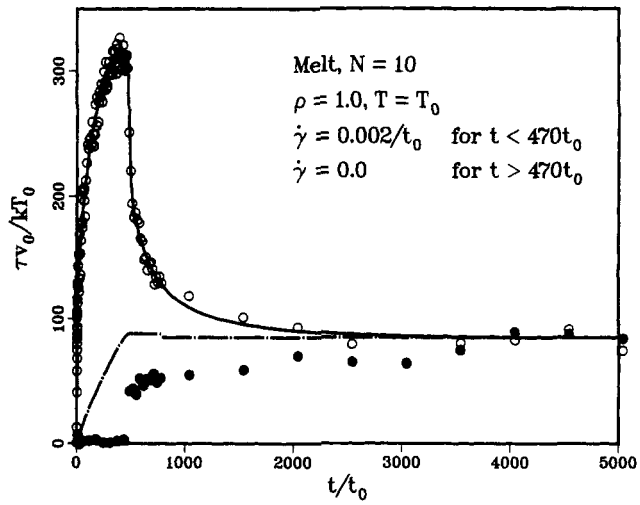

Figure 11. Stress relaxation in a model cross-linked system. After the melt is loaded for $t < t_1 = 470t_0$, all chain vectors are held fixed and $\dot{\gamma} = 0$ for $t > t_1$. Open circles denote $\tau(t)$ computed on the basis of the atomic virial stress formula, eq 8; filled circles denote $\tau(t)$ computed on the basis of eq 27 in terms of chain force $\mathbf{f}(\beta)$ determined by virial chain force formula, eq 28. Curves fitted to data on the basis of the Prony series, separately for $t < t_1$ and $t > t_1$. After time $t = 790t_0$, the simulation is continued for only 6 of the initial 120 configurations and data averaged over longer time periods in order to permit extension to longer times. The stress history denoted by the dash-dot line is computed on the basis of eq 27 in terms of ideal chain force $f(\beta)$. Minor irregularities in ideal stress history occur at a time when the number of initial configurations is reduced.

(5) Conclusions

We have conducted simulations by the method of molecular dynamics of the nonequilibrium viscoelastic behavior of an idealized model of a polymer melt. The stress is evaluated by means of the virial theorem, so that covalent and noncovalent (excluded-volume) interactions are treated on an equal footing.

An important conclusion that we draw from these studies is that the shear stress or anisotropic part of the stress arises principally from the excluded-volume interactions. This result is in strong contrast with the usual assumption that excluded-volume interactions make only an isotropic or hydrostatic contribution to the stress in such systems. It is in agreement, however, with what we have observed in earlier simulations of models for equilibrium rubber elasticity.

The assumption that excluded-volume interactions make only an isotropic contribution to the stress appears to be based on two premises:[20] the two-body excluded-volume potential is spherically symmetric, and the same is the case for the pair correlation function. In past work,[2,3] results of simulations of a polymeric system with an anisotropic chain vector distribution, as in a deformed network, indicate that the pair correlation function is no longer spherically symmetric because the excluded-volume interactions are screened through the action of the anisotropic covalent structure. This mechanism is consistent with both equilibrium and nonequilibrium conditions. In the present work, we see an additional mechanism for producing a nonspherically symmetric pair correlation function, namely the transient atomic ordering that occurs due to the interaction of packing requirements and an imposed time-dependent deformation. This mechanism is operative only under nonequilibrium conditions, but it is not dependent on the existence of a covalent structure and applies as well to a simple fluid.

In our studies on rubber elasticity we found that, although the physical method of stress production through screened excluded-volume interaction is very different from the classical picture that ascribes the stress to the chains acting as entropic springs in tension, the two approaches give numerical results in substantial agreement. For the present nonequilibrium simulations, the situation is very different. We find that the entropic spring mode of stress production greatly underestimates the actual stress produced by the excluded-volume interactions, particularly during the earlier stages of stress relaxation.

The contrast between the two modes of stress calculation is clearest in simulations in which the melt is first subjected to a shear strain by means of rapid ramp rise and then the strain and the chain vectors are held fixed (as though the melt is end cross-linked at the same instant that the strain becomes constant). Under these conditions, it is found that the stress based on the entropic force in the chains does not agree with the actual stress in the system until equilibrium is reached.

The entropic spring concept plays a central role in many theories of nonequilibrium stress relaxation.[21] Our simulations raise a serious question regarding the range of applicability of this concept in such processes. Consider first the glass modulus. It is highly insensitive to the degree of polymerization when all other factors, particularly the packing fraction, are held fixed. Under these conditions, it is also only very slightly dependent on the temperature. These insensitivities, observed experimentally as well as in our simulations, indicate that the concept of the entropic spring plays a very little role in the glassy regime. We may relate this to the fact that chains need time to explore all of the conformations available to them in order for the entropic force to take effect (see Figure 11 and the comparison between stress based on the ideal chain and

virial chain force). It is not yet completely clear at what point in the stress relaxation process the entropic spring becomes a meaningful concept. In our simulations of a model corresponding to a cross-linked system, this does not occur until the equilibrium rubber regime is reached. It might be argued that this is a consequence of the very short times required for relaxation in our model because of its high atomic mobility. However, it appears reasonable to expect that, as the atomic mobility decreases, the relaxation times and the time required for a chain to become entropic will increase in like proportion. This question clearly requires further study.

Of necessity, our simulations have dealt with idealized models with sufficient atomic mobility so that substantial stress relaxation takes place in reasonable time periods on the atomic time scale. In terms of the usual concept of time–temperature equivalence, we may think of our model as representing a system at very high temperature that exhibits an amount of stress relaxation on the atomic time scale equivalent to that which would take place at lower temperature on the laboratory time scale. The fact that our computed model parameters, when subjected to Caswell–Paboojian scaling, fall on the same curve as those for diverse polymeric systems gives us some confidence that the model results have relevance to real systems. They lead us to the conclusion that excluded-volume interactions play a central role in nonequilibrium viscoelastic processes in polymer melts.[22]

Acknowledgment. This work has been supported by the Gas Research Institute (Contract 5085-260-1152). The computations were performed on the Cray Y-MP at the Pittsburgh Supercomputer Center. We thank Bruce Caswell for supplying a preprint of ref 15 and for helpful discussions.

References and Notes

(1) Gao, J.; Weiner, J. H. *Macromolecules* **1989**, *22*, 979.
(2) Gao, J.; Weiner, J. H. *Macromolecules* **1991**, *24*, 1519.
(3) Gao, J.; Weiner, J. H. *Macromolecules* **1991**, *24*, 5179.
(4) See, for example: Ferry, J. D. *Viscoelastic Properties of Polymers*, 3rd ed.; Wiley: New York, 1980.
(5) Questad, D. L.; Pae, K.; Scheinbeim, J. J.; Newman, B. A. *J. Appl. Phys.* **1981**, *52*, 5977.
(6) See: Reference 4, p 268.
(7) Brown, D.; Clarke, J. H. R. *Macromolecules* **1991**, *24*, 2075.
(8) Berendsen, H.; Postma, J.; van Gunsteren, W. *J. Chem. Phys.* **1984**, *81*, 3684.
(9) Brown, D.; Clarke, J. H. R. *Comput. Phys. Commun.* **1991**, *62*, 368.
(10) Treloar, L. R. G. *The Physics of Rubber Elasticity*, 3rd ed.; Clarendon: Oxford, 1975; pp 84, 92, and 93. Note that there is a multiplicative factor of λ_1^2 omitted from eqs 5.21 and 5.22 on p 93 of this reference. See also: Love, A. E. H. *Mathematical Theory of Elasticity*, 4th ed.; Dover: New York, 1944; pp 33 and 34.
(11) Evans, D. J.; Morriss, G. P. *Statistical Mechanics of Nonequilibrium Liquids*; Academic Press: London, 1991; pp 133–146.
(12) Papanaastasiou, A. C.; Scriver, L.; Macosko, C. *J. Rheol.* **1983**, *27*, 387.
(13) Press, W. H.; Flannery, B. P.; Teukolsky, S. A.; Vetterling, W. T. *Numerical Recipes*; Cambridge University Press: Cambridge, 1986; pp 523–528.
(14) Alder, B. J.; Gass, D. M.; Wainwright, T. E. *J. Chem. Phys.* **1970**, *53*, 3813.
(15) Caswell, B.; Paboojian, S. J. *J. Rheol.*, preprint.
(16) For a good description of this ordering process as it applies to simple fluids subjected to a step shear deformation see Figure 1 in: Witten, T. A. *Phys. Today* **1990**, July, 21.
(17) See, for example: McQuarrie, D. A. *Statistical Mechanics*; Harper & Row: New York, 1976; p 258.
(18) Note that we are using the terminology of elastic and viscous parts of the stress as referring to the spring and dashpot contributions to a Maxwell body and not in the sense employed in: Doi, M.; Edwards, S. F. *The Theory of Polymer Dynamics*; Clarendon: Oxford, 1986; pp 220 and 221.
(19) The ideal chain force–length relation used is that appropriate for a freely-jointed chain of arbitrary length. See ref 2, eqs 9–11.
(20) See: Reference 18, pp 111 and 220.
(21) See, for example: reference 18, Chapter 7. Bird, R. B.; Curtiss, C. F.; Armstrong, R. C.; Hassager, O. *Dynamics of Polymeric Liquids, Kinetic Theory*, 2nd ed.; Wiley: New York, 1987; Vol. 2, Chapter 20 and further references cited therein.
(22) The same conclusion is reached in: Fixman, M. *J. Chem. Phys.* **1991**, *95*, 1410, a paper which came to our attention after the present manuscript was completed.